KSME

Springer

Journal of Mechanical Science and Technology 37 (2) 2023

Original Article
DOI 10.1007/s12206-023-0108-3

Keywords:
· Information fusion
· Particle filter algorithm
· Structural response reconstruction
· State space model
· Uncertainty

Correspondence to:
Zhenrui Peng
pzrui@163.com

Citation:
Shi, Y., Yin, H., Peng, Z., Wang, Z., Bai, Y. (2023). Structural response reconstruction based on the information fusion of multi-source particle filters. Journal of Mechanical Science and Technology 37 (2) (2023) 631~641. http://doi.org/10.1007/s12206-023-0108-3

Received July 18th, 2022
Revised October 13th, 2022
Accepted October 18th, 2022

† Recommended by Editor
No-cheol Park

Structural response reconstruction based on the information fusion of multi-source particle filters

Yonghe Shi[1], Hong Yin[1], Zhenrui Peng[1], Zenghui Wang[2] and Yu Bai[1]

[1]School of Mechanical Engineering, Lanzhou Jiaotong University, Lanzhou 730070, China,[2]School of Mechanical Engineering, Xi'an Jiaotong University, Xi'an 710049, China

Abstract Aiming at the problems that the lack of theoretical basis for the selection of particle set sampling variance and the resampling methods in traditional particle filter algorithms, and sampling process is easily disturbed by noise, an uncertainty structural response reconstruction method based on the information fusion of multi-source particle filters is proposed. Firstly, the sampling variance of particle set is analogous to the accuracy index of sensors, and a number of independent particle filtering samples from different sources are performed to ensure the independence of particles. Then, abnormal filters are screened and eliminated according to relative percentage error (RPE) threshold of preliminary reconstruction, and the state estimation results of remained particle filters are fused by the multi-source sensors information fusion technique to approximate to the real state values with high accuracy. Finally, the fused state values and the state space models are employed to reconstruct the responses of key positions, and the effectiveness of the proposed method is verified by numerical example of the space truss structure and the cantilever beam test. The results show that the proposed method can reduce the influence of the above uncertainties on reconstruction results, effectively improve the particle impoverishment problem, the filtering stability is good and the reconstruction accuracy is high.

1. Introduction

In engineering, the response data collected by sensors is the basis for structural dynamic analysis, especially for health monitoring techniques in the structural safety assessment [1, 2], where the completeness of measurement data directly influences the structural performance evaluation. However, due to the complexity of actual engineering structures, the position and the number of measurement points are limited by economic conditions and installation conditions. It is difficult to obtain complete measurement data. Therefore, the structural response reconstruction technique, which uses the limited measurement data to reconstruct the responses at the positions which are difficult to measure or where sensors are missing or damaged, is of great research significance [3, 4].

At present, structural response reconstruction techniques are divided into the two main categories: the deterministic method and the uncertainty method. The former mainly includes the empirical modal decomposition method [5, 6], the transmissibility method [7, 8], and the modal analysis method [9], etc. The prerequisite for the application of deterministic methods is to establish a finite element model with high accuracy, but it is hard to establish an accurate finite element model for the actual engineering structure, which greatly limits the application of deterministic methods. The later can reduce the influence of modeling errors and measurement noise on the response reconstruction, which is mainly based on the Kalman filter (KF) algorithm [10]. Zhang et al. [11] proposed a method based on KF algorithm for the optimal arrangement of multi-type sensors, and reconstructed the responses of key nodes using the measurement data. Dong et al. [12] proposed a sensor optimization method based on meta-heuristic. Fortu-

nately, the particle filter (PF) algorithm [15] cannot only perform well in the non-linear and non-Gaussian system, but can handle the colored noise better. But it was found that the traditional PF algorithm is susceptible to uncertainties and suffers from particle impoverishment and particle degradation problems [16]. In recent years, scholars have also carried out related researches on the improvement and application of PF algorithm [17-20], but most of the researches are aimed at the sampling radius of a single particle set. It should be noted that the sampling radius of particle set is a key factor to the state estimation accuracy. When sampling radius is different, the spatial range of particle distribution is also different, and the filtering results will occur corresponding deviations. When sampling radius is too small, the obtained particles will quickly concentrate on a certain value, that is, the "tight" distribution of particles and the number of true state values will drop rapidly. When sampling radius is too large, the "loose" distribution of particle is easy to occur, resulting in the sample points cannot fully reflect their real state properties. At the same time, the resampling method is also the key factor affecting the sampling quality [21]. Particle sets are reorganized by eliminating the particle with small weight to improve the particle degradation problem. However, the selection of resampling methods often lacks the theoretical basis, resulting in poor filtering effect.

Fortunately, information fusion technique [22-27] can fully consider the influence of the above uncertainties, such as the modeling errors, sampling radius of particle set, and resampling method. It can synthesize the multi-source data by mathematical analysis and computer technique, and improve the information quality and reduce the impact of uncertainties using the complementarity of multi-source data. The purpose of information fusion estimation is to perform a comprehensive processing on different observation vectors to obtain a more accurate state parameter vector than the original observation vector, which can avoid the problem of improper selection of sampling variance and sampling method of particle set. Thus, the information fusion technique is adopted to the response reconstruction process to obtain the high-quality state estimation result.

In the above context, a new structural response reconstruction method based on the information fusion technique and the multi-source particle filters is proposed in this paper. Firstly, PF algorithm is introduced to design and implement the multiple independent particle filter sampling process. The initial response reconstruction is carried out and abnormal particle filter is eliminated according to the relative percentage error (RPE) threshold. To obtain high-quality state estimates, the multi-source sensors grouping weighted fusion algorithm is introduced to fuse the state estimates from the screened particle filters. Then, the fused state result is adopted to response reconstruction to reduce the influence of uncertainties and to improve the particle impoverishment problem. Finally, the effectiveness of the proposed method is verified by numerical example of the space truss and the cantilever beam test.

The rest of the paper is organized as follows. In Sec. 2, the state space model theory and PF algorithm are discussed. In Sec. 3 the multi-source sensors grouping weighted information fusion algorithm, reconstruction equation, and our multi-source particle filters information fusion scheme is presented in detail. Sec. 4 shows the results of two cases. Finally, Sec. 5 concludes the manuscript.

2. Theoretical basis

2.1 State space model

The second-order dynamic equation for the structural system can be expressed in the modal coordinate system as

$$\ddot{\boldsymbol{q}} + 2\boldsymbol{\xi}\boldsymbol{\omega}_0\dot{\boldsymbol{q}} + \boldsymbol{\omega}_0^2\boldsymbol{q} = \boldsymbol{\Phi}^{\mathrm{T}}\boldsymbol{L}\boldsymbol{u} \tag{1}$$

where $\boldsymbol{q}$ is the modal coordinate; $\boldsymbol{\xi}$ is the damping matrix; $\boldsymbol{\omega}_0$ is the modal frequency matrix; $\boldsymbol{\Phi}$ is the displacement mode shape matrix; $\boldsymbol{L}$ is the mapping matrix of excitation load; $\boldsymbol{u}$ is the external excitation vector in modal coordinate system.

Transforming Eq. (1) into state space model and discretizing it, the process can be expressed as

$$\begin{cases} \boldsymbol{x}_{k+1} = \boldsymbol{A}\boldsymbol{x}_k + \boldsymbol{B}\boldsymbol{u}_k + \boldsymbol{a}_k \\ \boldsymbol{y}_k = \boldsymbol{C}\boldsymbol{x}_k + \boldsymbol{D}\boldsymbol{u}_k + \boldsymbol{v}_k \end{cases} \tag{2}$$

where $\boldsymbol{x}_k$ is the discrete state vector; $\boldsymbol{y}_k$ is the discrete observation vector; $\boldsymbol{u}_k$ is the discrete external excitation vector; $\boldsymbol{A}$ and $\boldsymbol{B}$ are the discrete state matrix and the external excitation input matrix, respectively; $\boldsymbol{C}$ and $\boldsymbol{D}$ are the observation output matrix and the direct transmission matrix, respectively; $\boldsymbol{a}_k$ is the process noise of the system to account for errors due to modelling uncertainties; $\boldsymbol{v}_k$ is the measurement noise of sensors. The matrices in the state transfer equation can be expressed as

$$\boldsymbol{x}_k = \begin{bmatrix} \boldsymbol{q}_k \\ \dot{\boldsymbol{q}}_k \end{bmatrix} \tag{3}$$

$$\boldsymbol{A} = \mathrm{e}^{\begin{bmatrix} 0 & \boldsymbol{I} \\ -\boldsymbol{\omega}_0^2 & -2\boldsymbol{\xi}\boldsymbol{\omega}_0 \end{bmatrix}\Delta t} \tag{4}$$

$$\boldsymbol{B} = \begin{bmatrix} 0 & \boldsymbol{I} \\ -\boldsymbol{\omega}_0^2 & -2\boldsymbol{\xi}\boldsymbol{\omega}_0 \end{bmatrix}^{-1} (\boldsymbol{A} - \boldsymbol{I}) \begin{bmatrix} 0 \\ \boldsymbol{\Phi}^{\mathrm{T}}\boldsymbol{L} \end{bmatrix}. \tag{5}$$

$\boldsymbol{C}$ and $\boldsymbol{D}$ of the observation equation are related to the signal category being observed. When the observation categories are displacement and acceleration, $\boldsymbol{C}$ and $\boldsymbol{D}$ can be expressed as

$$\boldsymbol{C} = \begin{bmatrix} \boldsymbol{\Phi} & 0 \\ -\boldsymbol{\Phi}\boldsymbol{\omega}_0^2 & -2\boldsymbol{\Phi}\boldsymbol{\xi}\boldsymbol{\omega}_0 \end{bmatrix} \quad \boldsymbol{D} = \begin{bmatrix} 0 \\ \boldsymbol{\Phi}\boldsymbol{\Phi}^{\mathrm{T}}\boldsymbol{L} \end{bmatrix}. \tag{6}$$

2.2 Particle filtering

Particle filtering is an approximate Bayesian filtering algorithm based on the Monte Carlo simulation, which can be employed to any state space model. The core of PF algorithm is to represent the posterior probability density function of the system state by the discrete random samples with weight.

PF algorithm takes a set of random samples with corresponding weight from the prior probability distribution to approximate the posterior probability density function, transforms the integration operation into the summation operation over a finite number of samples, and performs the weighting and the recursive operation according to the Bayesian criteria to obtain the system state estimation. This process can be expressed as

$$\begin{cases} \boldsymbol{x}_{k+1} = f\left(\boldsymbol{x}_k\ ,\ \boldsymbol{a}_{k+1}\right) \\ \boldsymbol{y}_{k+1} = g\left(\boldsymbol{x}_{k+1}\ ,\ \boldsymbol{v}_{k+1}\right) \end{cases} \tag{7}$$

where $\boldsymbol{x}_{k+1}$ is the state vector at k+1 moment; $f(\cdot)$ is the system state equation, representing the relational function of state vector iterative from the k moment to the k+1 moment; $\boldsymbol{a}_{k+1}$ is the system process noise; $\boldsymbol{y}_{k+1}$ is the observation vector; $g(\cdot)$ is the system observation equation, representing the relational function of the transformation from the state vector at k moment to the observation vector at k+1 moment; $\boldsymbol{v}_{k+1}$ is the measurement noise of sensors.

It is assumed that the system state conforms to the Markov process [13], that is, the current state is only related to the previous state. Firstly, the prior probability distribution of the system state at k moment is obtained by the prediction step, and the system state prediction equation can be expressed as

$$p\left(\boldsymbol{x}_k \left| \boldsymbol{y}_{1:k-1}\right.\right) = \int p\left(\boldsymbol{x}_k \left| \boldsymbol{x}_{k-1}\right.\right) p\left(\boldsymbol{x}_{k-1} \left| \boldsymbol{y}_{1:k-1}\right.\right) \mathrm{d}\boldsymbol{x}_{k-1} . \tag{8}$$

Then, combining the observation values $\boldsymbol{y}_k$ at k moment, the posterior probability distribution of the system state is obtained by the updating step. The updating equation of system state is

$$p\left(\boldsymbol{x}_k \left| \boldsymbol{y}_{1:k}\right.\right) = \frac{p\left(\boldsymbol{y}_k \left| \boldsymbol{x}_k\right.\right) p\left(\boldsymbol{x}_k \left| \boldsymbol{y}_{1:k-1}\right.\right)}{p\left(\boldsymbol{y}_k \left| \boldsymbol{y}_{1:k-1}\right.\right)} \tag{9}$$

$$p\left(\boldsymbol{y}_k \left| \boldsymbol{y}_{1:k-1}\right.\right) = \int p\left(\boldsymbol{y}_k \left| \boldsymbol{x}_k\right.\right) p\left(\boldsymbol{x}_k \left| \boldsymbol{y}_{1:k-1}\right.\right) \mathrm{d}\boldsymbol{x}_k . \tag{10}$$

The prior probability distribution $p\left(\boldsymbol{x}_k \left| \boldsymbol{y}_{1:k-1}\right.\right)$ is calculated by the posterior probability distribution $p\left(\boldsymbol{x}_{k-1} \left| \boldsymbol{y}_{1:k-1}\right.\right)$, the transfer probability density $p\left(\boldsymbol{x}_k \left| \boldsymbol{x}_{k-1}\right.\right)$, and the state prediction equation. Then, the posterior probability distribution $p\left(\boldsymbol{x}_k \left| \boldsymbol{y}_{1:k}\right.\right)$ is calculated by the prior probability distribution of the current state and the state updating equation.

In solving the posterior probability distribution, the standard PF algorithm combines Monte Carlo simulation and sequential importance sampling methods to solve the problem of high-dimensional integration and the difficulty of sampling in the posterior distribution. The easily implemented prior probability density function is selected as the importance function, which can be expressed as

$$\pi\left(\boldsymbol{x}_k \left| \boldsymbol{x}_{0:k-1}\ ,\ \boldsymbol{y}_{1:k}\right.\right) = p\left(\boldsymbol{x}_k \left| \boldsymbol{x}_{k-1}\right.\right) . \tag{11}$$

The posterior distribution, also known as the state transfer equation, obtained by estimating after importance sampling can be expressed as

$$p\left(\boldsymbol{x}_k \left| \boldsymbol{y}_{0:k}\right.\right) \approx \sum_{i=1}^{N} \boldsymbol{w}_k^i \delta\left(\boldsymbol{x}_k - \boldsymbol{x}_k^i\right) . \tag{12}$$

On the basis of the first-order Markov assumption, the weight recurrence form can be simplified as

$$\begin{aligned} \boldsymbol{w}_k &= \boldsymbol{w}_{k-1} \frac{p\left(\boldsymbol{y}_k \left| \boldsymbol{x}_k\right.\right) p\left(\boldsymbol{x}_k \left| \boldsymbol{x}_{k-1}\right.\right)}{\pi\left(\boldsymbol{x}_k \left| \boldsymbol{x}_{0:k-1}\ ,\ \boldsymbol{y}_{1:k}\right.\right)} \\ &= \boldsymbol{w}_{k-1} \frac{p\left(\boldsymbol{y}_k \left| \boldsymbol{x}_k\right.\right) p\left(\boldsymbol{x}_k \left| \boldsymbol{x}_{k-1}\right.\right)}{p\left(\boldsymbol{x}_k \left| \boldsymbol{x}_{k-1}\right.\right)} \end{aligned} \tag{13}$$

$$\boldsymbol{w}_k^{(i)} = \boldsymbol{w}_{k-1}^{(i)} p\left(\boldsymbol{y}_k \left| \boldsymbol{x}_k^{(i)}\right.\right) . \tag{14}$$

3. Structural response reconstruction

3.1 Multi-source sensors information fusion algorithm

Information fusion technique uses the complementarity of multi-source data to reduce the influence of uncertainties, which can improve the fault tolerance of system while ensuring the information confidence, and is widely used in the state estimation field. Therefore, the information fusion technique is introduced to improve the state estimation accuracy, which can get the better result which is difficult to obtain by a single filter.

At present, there are many kinds of sensor information fusion algorithms, such as the probabilistic methods, neural networks, and group weighting fusion methods, etc. Among them, the group weighted fusion algorithm is more mature, with unbiased, real-time, and simple numerical operation, thus the multi-sensors group weight fusion algorithm is introduced to perform the fusion of multi-source filters.

Assuming n sensors, the observation equation of the system state can be expressed as

$$\boldsymbol{y} = \boldsymbol{h}x + \boldsymbol{\vartheta} \tag{15}$$

where x is state quantity to be measured, represents a state value to be measured; $\boldsymbol{h} = (1\,1 \cdots 1)^{\mathrm{T}}$ is the n-dimensional drive constant vector; $\boldsymbol{y} = (y_1\ y_2 \cdots y_n)^{\mathrm{T}}$ is the measurement vector. $\boldsymbol{\vartheta} = (\vartheta_1\ \vartheta_2\ \cdots\ \vartheta_n)$ is an n-dimensional error vector, containing redundant information of the sensor, namely the internal noise of the sensor and environmental interference

noise. Assuming that the redundant information from each sensor is independent of each other and follows a normal distribution, thus $\vartheta_i \sim N(0, R_i)$, $R_i (i = 1\,2 \cdots n)$ is the measurement variance of the *i*-th sensor.

The sensors are randomly divided into *m* groups, and the number of sensors in each group must meet the request that $p \geq 2$, and the measurement average $\bar{y}_i$ of each group sensors is used to replace the multiple sensors in the group to participate in information fusion.

$$\bar{y}_i = \frac{1}{n_i} \sum_{j=1}^{n_i} y_{ij} \quad i = 1, 2, \cdots, m \tag{16}$$

where y_{ij} is the measured value of the *j*-th sensor in the *i*-th group.

Thus, the observation equation of the system state can be described by the measurement mean values of all groups. Eq. (15) can be further expressed as

$$\bar{\boldsymbol{y}} = \bar{\boldsymbol{h}} x + \bar{\boldsymbol{\vartheta}} \tag{17}$$

where $\bar{\boldsymbol{y}} = (\bar{y}_1 \ \bar{y}_2 \ \cdots \bar{y}_m)^{\mathrm{T}}$ is the measurement mean vector of *m* groups sensors; $\bar{\boldsymbol{h}}$ is the *n*-dimensional drive constant vector; and $\bar{\boldsymbol{\vartheta}}$ is the *n*-dimensional error mean vector. Since the sum of mutually independent normal distributions still obeys normal distribution, thus $\bar{\vartheta}_i \sim N(0, \bar{R}_i)$, $\bar{R}_i (i = 1\,2 \cdots m)$ is the mean value of the measurement variance of the *i*-th group of sensors, thus, $\bar{\boldsymbol{y}}_i \sim N(x, \bar{R}_i)$, and $\bar{\boldsymbol{y}}_i (i = 1\,2 \cdots m)$ is independent of each other, so $\bar{\boldsymbol{y}} \sim N(\bar{\boldsymbol{h}} x, \bar{\boldsymbol{R}})$.

Under the condition of measuring the state variable x, the probability density of $\bar{\boldsymbol{y}}$ can be expressed as a function of x, and the corresponding likelihood function can be expressed as [28]

$$L(\bar{\boldsymbol{y}} | x) = -\frac{m}{2} \ln(2\pi) - \frac{1}{2} \ln(\det \bar{\boldsymbol{R}}) - \frac{1}{2} (\bar{\boldsymbol{y}} - \bar{\boldsymbol{h}} x)^{\mathrm{T}} \bar{\boldsymbol{R}}^{-1} (\bar{\boldsymbol{y}} - \bar{\boldsymbol{h}} x) \tag{18}$$

where $\bar{\boldsymbol{R}} = \mathrm{diag}(\bar{R}_1 \ \bar{R}_2 \ \cdots \ \bar{R}_m)$ is the variance matrix of each group measurement; $\bar{R}_i (i = 1\,2 \cdots m)$ is the mean value of measurement variance of the *i*-th group. Maximizing the likelihood function $L(\bar{\boldsymbol{y}} | x)$ to obtain an estimation state $\hat{x}$, which is also the weighted fusion formula of the mean measurement.

$$\hat{x} = (\bar{\boldsymbol{h}}^{\mathrm{T}} \bar{\boldsymbol{R}}^{-1} \bar{\boldsymbol{h}})^{-1} \bar{\boldsymbol{h}}^{\mathrm{T}} \bar{\boldsymbol{R}}^{-1} \bar{\boldsymbol{y}} = \frac{\sum_{i=1}^{m} \frac{1}{\bar{R}_i} \bar{y}_i}{\sum_{i=1}^{m} \frac{1}{\bar{R}_i}}. \tag{19}$$

To consider the process properties of the measurement variance for each group, the group variance estimation learning algorithm [21] is employed to dynamically and recursively obtain the real-time measurement variance of each group, which can be expressed as

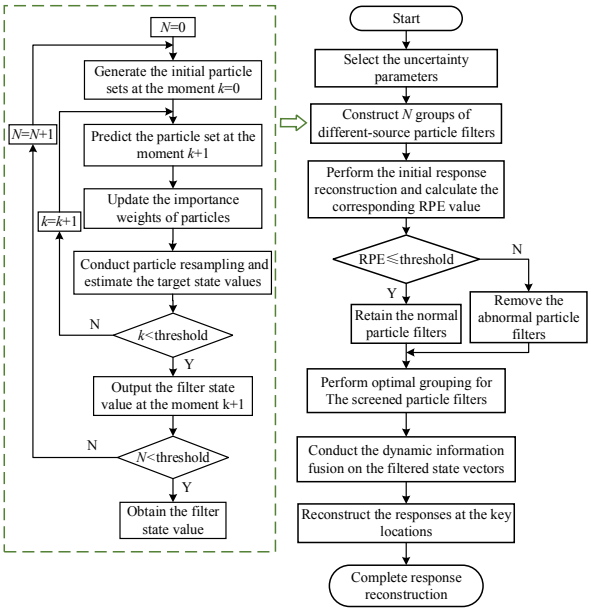

Fig. 1. Flow chart of structural response reconstruction.

$$\bar{R}_i^{(m)} = \frac{m-1}{m} \bar{R}_i^{(m-1)} + \frac{1}{m} \bar{R}_i^{(m)} \quad m = 1, 2, \cdots \tag{20}$$

where $\bar{R}_i^{(m)}$ is the measurement variance of sensors in the *i*-th group at the *m*-th measurement. Let the measurement variance in the *i*-th group at the first measurement be $\bar{R}_i^{(0)} = 0$, substitute Eq. (20) into Eq. (19) to obtain the fusion state $\hat{x}$ at the *m*-th sampling.

3.2 Reconstruction equations

The responses of key structural positions can be reconstructed by discrete state space model, and the fused predictive state vector obtained by multi-source sensors information fusion method in Sec. 3.1, which can be expressed as

$$\begin{cases} \boldsymbol{y}_k^e = \boldsymbol{C}_r \hat{\boldsymbol{x}}_k + \boldsymbol{D}_r \boldsymbol{u}_k \\ \boldsymbol{y}_k^r = \boldsymbol{C}_r \boldsymbol{x}_k + \boldsymbol{D}_r \boldsymbol{u}_k \end{cases} \tag{21}$$

where $\boldsymbol{y}_k^e$ and $\boldsymbol{y}_k^r$ are the fused reconstructed responses and the true computed responses, respectively; $\boldsymbol{C}_r$ and $\boldsymbol{D}_r$ are the submatrices of $\boldsymbol{C}$ and $\boldsymbol{D}$, respectively; $\boldsymbol{C}_r$ is the observed output matrix; $\boldsymbol{D}_r$ is the direct transmission matrix; $\boldsymbol{x}_k$ is the computed state vector; $\hat{\boldsymbol{x}}_k$ is the fused state vector.

The displacement and acceleration responses at key positions can be reconstructed by the following equation

$$\boldsymbol{y}_k^e = \begin{bmatrix} \boldsymbol{d}_k \\ \boldsymbol{a}_k \end{bmatrix} = \begin{bmatrix} \boldsymbol{\Phi} & 0 \\ -\boldsymbol{\Phi}\boldsymbol{\omega}_0^2 & -2\boldsymbol{\Phi}\boldsymbol{\xi}\boldsymbol{\omega}_0 \end{bmatrix} \hat{\boldsymbol{x}}_k + \begin{bmatrix} 0 \\ \boldsymbol{\Phi}\boldsymbol{\Phi}^{\mathrm{T}} \boldsymbol{L} \end{bmatrix} \boldsymbol{u}_k. \tag{22}$$

The widely used relative percentage error (RPE) is introduced to test the accuracy of reconstruction results, which can

be expressed as

$$\mathrm{RPE}=\frac{\mathrm{std}(\boldsymbol{y}^{e}-\boldsymbol{y}^{r})}{\mathrm{std}(\boldsymbol{y}^{r})}\times 100\% \tag{23}$$

where std is the standard deviation; $\boldsymbol{y}^{e}$ is the reconstructed response vector; $\boldsymbol{y}^{r}$ is the true response vector.

The specific process of structural response reconstruction based on the fusion information of multi-source particle filters is shown in Fig. 1.

4. Illustrative examples

4.1 Analytical problem: simulation analysis of the space truss

The space truss structure widely used in engineering is employed to test the response reconstruction process. The truss structure is divided into three parts: the upper chord, the web rod (straight rod and diagonal rod), and the lower chord, and the basic parameters are listed in Table 1. The truss structure consists of 66 rod units with 28 nodes, which are articulated. Vibrations only in Y and Z directions are considered at each node and the four support nodes are fixedly constrained, the whole structure has 48 degrees of freedom and its specific node numbers are shown in Fig. 2.

The random white noise excitation is applied in Y-direction at the 26th node of the space truss structure to simulate the random excitation at mid-span position. In general, the lower modes contain the main information of the structure, reflecting the dynamic behavior of the structure. Therefore, the first 6 orders of modal frequencies are used for reconstruction. The frequencies are 18.19 Hz, 30.90 Hz, 50.58 Hz, 70.97 Hz, 90.06 Hz, and 95.21 Hz. Considering the structural constraints of the truss structure, that is, the positions of its nodes 17, 22, 23, and 28 (referred to as the key nodes) are difficult to install sensors. Thus, the displacement and acceleration responses of the above key nodes are reconstructed by the acceleration responses at 8 nodes: 2, 7, 10, 15, 18, 21, 24, and 27, which are easy to measure. At the same time, considering that the Gaussian white noise assumption is difficult to meet the engineering reality, so the 3 % colored noise is added to the calculated responses to simulate the measured responses, and its spectrum is shown in Fig. 3.

Table 1. Basic parameters of the space truss structure.

Rod units	Elastic modulus /(GPa)	Density /(kg/m^3)	Cross-sectional area/(mm^2)
Top chords	285	7800	85.5
Straight rods	380	7800	141.0
Diagonal rods	380	7800	45.0
Lower chords	228	7800	85.5

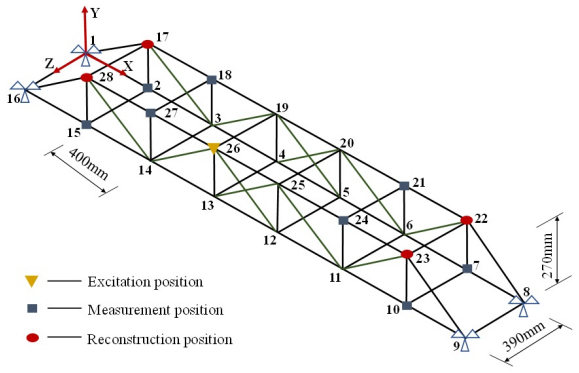

Fig. 2. Space truss model.

It can be seen from the previous section, the sampling radius of particle set determines the state estimation accuracy, which is also known as the sampling variance of particle set (*SVPS*). It can be given by the following expression

$$SVPS=Q\cdot \mathrm{sqrt}(\hat{\boldsymbol{x}}_k)\cdot \boldsymbol{Ra} \tag{24}$$

where Q is the control coefficient, which is used to adjust the sampling radius of particle set; $\hat{\boldsymbol{x}}_k=(\bar{x}_{k1}\ \bar{x}_{k2}\ \cdots\ \bar{x}_{kn})^{\mathrm{T}}$ is the base state vector, consisting of the mean magnitude order of each calculated state component; $\boldsymbol{Ra}$ is the random matrix obeying Gaussian distribution.

To fully consider the influence of uncertainties due to resam-

Table 2. Parallel experimental design of filters.

Classification	Filter number	Experimental design
Resampling methods	1	System resampling
	2	Polynomial resampling
	3	Residual resampling
SVPS control coefficient	4	Q = 6×10^{-3}
	5	Q = 4×10^{-3}
	6	Q = 3×10^{-3}
	7	Q = 2×10^{-3}
	8	Q = 1×10^{-3}

Note: Q is used to control the sampling radius of the particle set, the larger the value the looser the particles, the smaller the particles are tighter; the first three sets of filters have parameters Q = 1×10^{-3}, the last five sets of filters for random resampling.

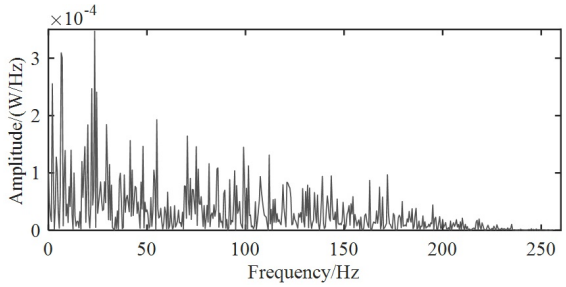

Fig. 3. Spectrum of colored noise.

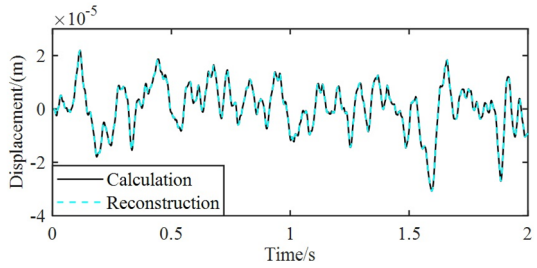

(a) Displacement in Y direction at the 17th node

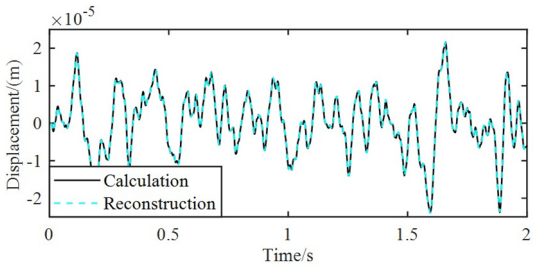

(b) Displacement in Y direction at the 22nd node

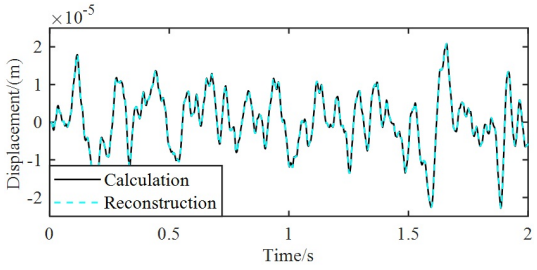

(c) Displacement in Y direction at the 23rd node

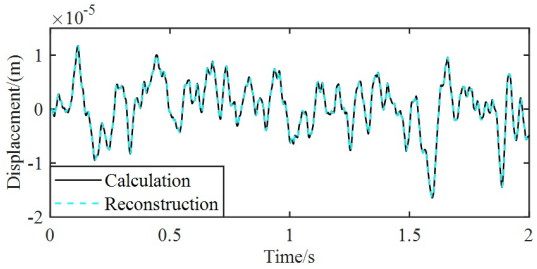

(d) Displacement in Y direction at the 28th node

Fig. 4. Fused reconstruction results of displacement.

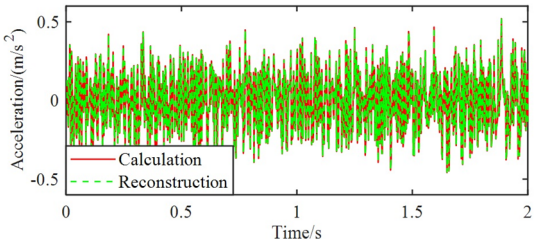

(a) Acceleration in Y direction at the 17th node

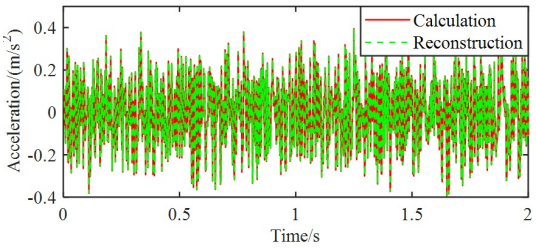

(b) Acceleration in Y direction at the 22nd node

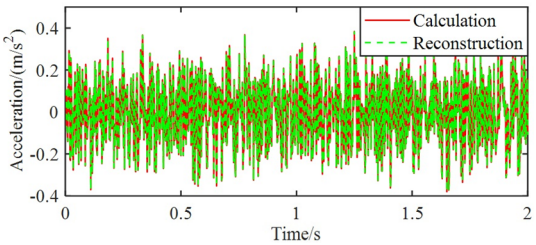

(c) Acceleration in Y direction at the 23rd node

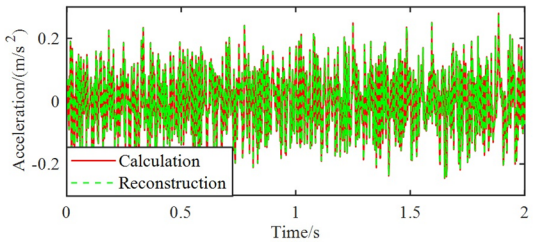

(d) Acceleration in Y direction at the 28th node

Fig. 5. Fused reconstruction results of acceleration.

pling methods and sampling radius of particle set in traditional PF algorithms, the experimental design of filters is carried out. Firstly, the results of the preliminary response reconstruction are analyzed, and the approximate interval of the *SVPS* control factor corresponding to the convergence of the reconstruction is determined, and then the *SVPS* control factor of the filter is randomly obtained in the interval. The specific design scheme is listed in Table 2.

In addition, abnormal filters can affect the final fusion results and even lead to the scattered fusion result. Therefore, before the information fusion, the filters are screened through the displacement RPE threshold, and if the RPE is larger than 5 %, the filters are judged as abnormal filters and are eliminated, otherwise, they are retained. Then, the mean displacement at each key node is used as the indicator to optimally group the remained filters according to the optimal grouping principle [22]. The information fusion of state estimates is performed by Eqs. (19) and (20).

The displacement and the acceleration responses at key nodes 17, 22, 23, and 28 are reconstructed by the fused state results and the state space model, the reconstructed results are shown in Figs. 4 and 5, respectively. It can be seen that the reconstructed displacement and acceleration responses at nodes 17, 22, 23, and 28 can fit well with the real responses, which indicates that the proposed method can reconstruct the structural responses of key nodes with high accuracy.

To verify the effectiveness of the proposed method, the RPE values of single filter reconstruction methods and the proposed method are calculated and compared, and the results are

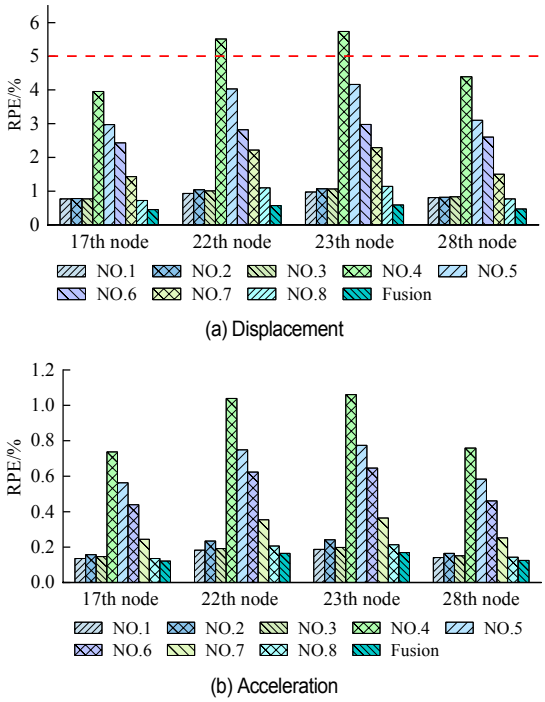

(a) Displacement

(b) Acceleration

Fig. 6. Relative percentage errors of key nodes.

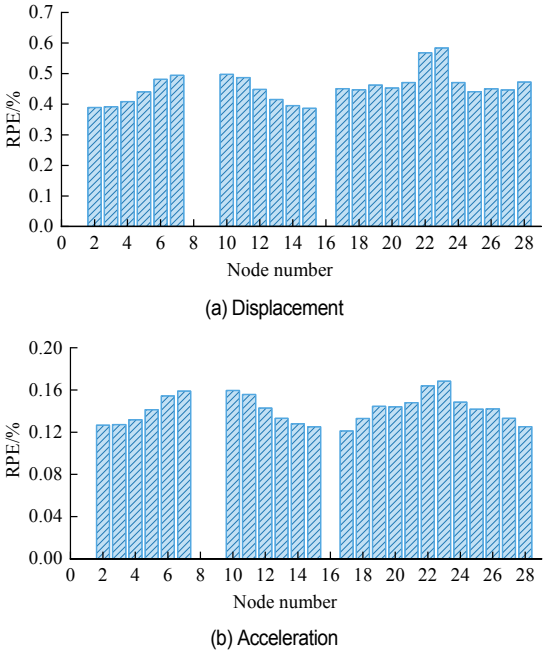

(a) Displacement

(b) Acceleration

Fig. 7. Relative percentage errors at all nodes.

shown in Fig. 6. It can be clearly seen that the RPE values by the proposed fusion reconstruction method are significantly lower than those by the other signal filter methods, and the reconstruction accuracy by the proposed method is significantly better than that by the standard PF algorithm.

To further verify the stability of the proposed method, the RPE values of fused reconstruction results for displacement

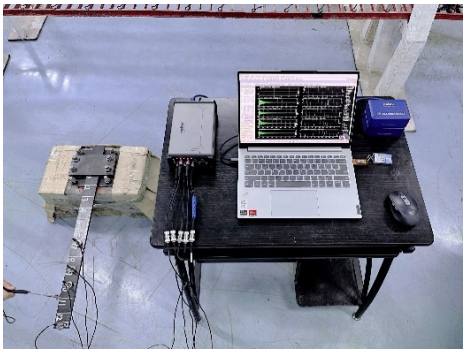

(a) Actual structure of the cantilever beam

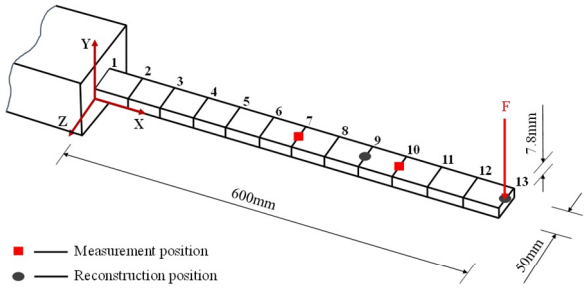

(b) Finite element model of the cantilever beam

Fig. 8. Cantilever beam.

and acceleration at all nodes are calculated, and the results are shown in Fig. 7. It can be seen that the RPE values at nodes 1, 8, 9, and 16 are zeros due to their fixed constraints, and the RPE values of displacements and accelerations at remaining nodes are lower than 0.6 % and 0.2 %, respectively, indicating the robustness of the proposed method.

4.2 Engineering problem: cantilever beam test

In actual engineering analysis, many engineering machinery components can be simplified as cantilever beams, which dynamic characteristics directly affect the structural stability. Therefore, the proposed method is experimentally verified by the cantilever beam structure as shown in Fig. 8(a).

The main design material parameters are that the mass density is 6440 $kg \cdot m^{-3}$ and the modulus of elasticity is 128 GPa. The cantilever beam is divided into 12 units and only the Y-directional degree of freedom at each unit node are considered. In practical engineering, the end position of the cantilever beam, that is the node 13, vibrates most severely when subjected to external forces. Therefore, a hammering excitation is applied at the node 13, and the responses at nodes 9 and 13 are reconstructed by the responses at 2 nodes, 7 and 10. The specific excitation ***F*** and node positions to be reconstructed are shown in Fig. 8(b).

The test is performed by the INV3062-C2(L) network distributed acquisition instrument system and the DASP-v11 signal analysis software package, which are used to complete the acceleration signal acquisition and the modal analysis. By applying the vertical excitation to cantilever beam using the MSC-

Table 3. Parallel experimental design of filters.

Classification	Filter number	Experimental design
Resampling methods	1	System resampling
	2	Polynomial resampling
	3	Residual resampling
SVPS control coefficient	4	$Q = 5\times10^{-4}$
	5	$Q = 5\times10^{-3}$
	6	$Q = 1\times10^{-3}$
	7	$Q = 5\times10^{-2}$
	8	$Q = 1\times10^{-2}$

Note: The first three sets of filters have parameters $Q = 1\times10^{-2}$ and the last five sets of filters for random resampling.

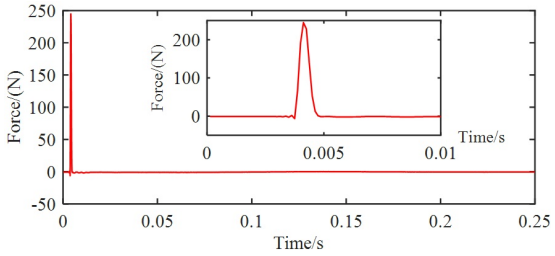

Fig. 9. Time history curve of the excitation.

3 elastic force hammer, the acquisition system records both the excitation force signal and the acceleration signal at measurement points, and subsequently identifies modal responses such as frequencies and mode shapes of the structure using the DASP software package. The first five-order modal frequencies are 20.39 Hz, 121.32 Hz, 342.33 Hz, 657.43 Hz, and 1080.88 Hz, respectively, and the time-history curve of the excitation is shown in Fig. 9.

To reduce the effects of uncertainties including resampling methods and sampling variances of particle sets, the filters are designed as listed in Table 3. Due to the actual measurement errors, the filters are eliminated by the acceleration RPE threshold MAX = 50 %, then the response reconstruction is carried out according to the flow shown in Fig. 1.

The acceleration responses at nodes 9 and 13 of cantilever beam are reconstructed using the fused state results and the state space model. The time-history fitting curves are shown in Figs. 10(a) and (b), respectively. It can be seen that the measured responses at nodes 9 and 13 are basically close to the reconstructed responses obtained by the proposed method.

The fitted curves of the Fourier spectrum amplitudes for acceleration responses at the node 9 and the node 13 of cantilever beam are shown in Figs. 11(a) and (b), respectively. It can be seen that the Fourier amplitudes of the reconstructed acceleration and the measured acceleration maintain good agreement, which indicates that the proposed method can reconstruct the structural responses with high accuracy.

To further verify the effectiveness of the proposed method, RPE values of the single filter methods and the proposed method are calculated and compared, respectively, and the

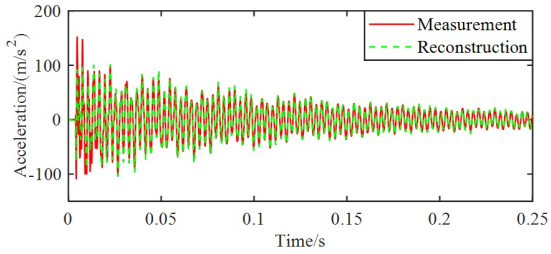

(a) Acceleration at the 9th node

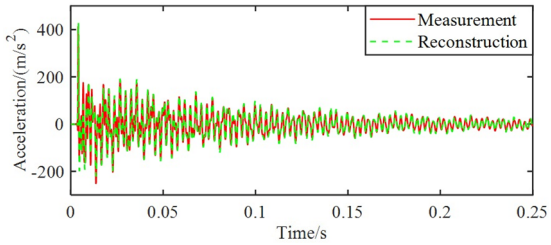

(b) Acceleration at the 13rd node

Fig. 10. Fused reconstruction results of acceleration.

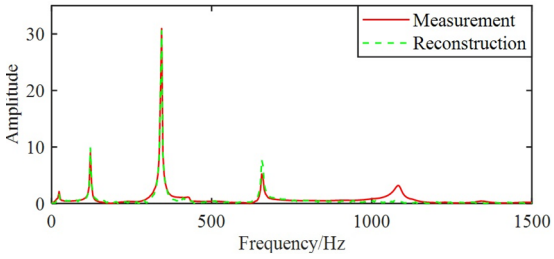

(a) 9th node

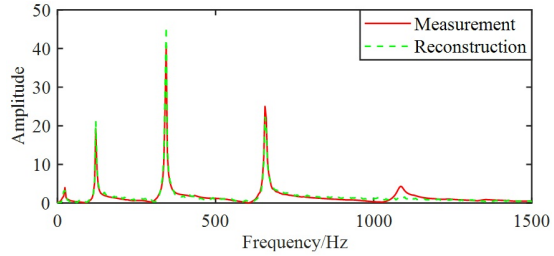

(b) 13rd node

Fig. 11. Fourier spectrum of acceleration.

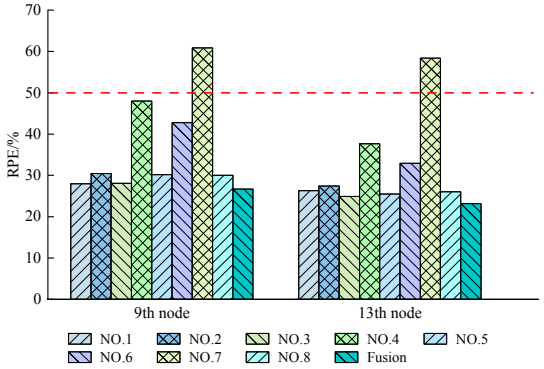

Fig. 12. Relative percentage errors of key nodes.

results are shown in Fig. 12.

It can be clearly seen that the RPE of the reconstruction results based on information fusion are significantly lower than those of single filter methods, indicating that the proposed method can reconstruct the responses at difficult measurement positions more stably, and the fused reconstruction results are more accurate than those of the single filter, and have a certain degree of error tolerance.

5. Conclusion

A new structural response reconstruction method based on the information fusion of multi-source particle filters is proposed. The following conclusions are mainly obtained:

1) The introduction of information fusion technique can effectively reduce the influence of uncertainties such as the sampling variance of particle set and the improper selection of resampling methods, which provides a new idea for solving the problem of uncertainty structural response reconstruction.

2) The proposed method can increase the diversity of particles and improve the particle impoverishment problem while ensuring better reconstruction accuracy. At the same time, it can effectively avoid the tight and the loose distribution of particles in single-filter methods.

3) It can maintain good reconstruction results even in the case of colored noise pollution, and has good fault tolerance, which has certain reference value for engineering practice.

The method proposed in this paper requires the external excitation of the known structure. In view of the problem that the load is difficult to obtain in the actual situation, the author will focus on Bayesian theory to further solve the problem of unknown load in the future research.

Acknowledgments

This work is supported by the National Natural Science Foundation of China (No:62161018); the Natural Science Foundation of Gansu Province (20JR10RA234); and the Outstanding Graduate Student “Innovation Star” Project of Gansu Province (2022CXZX-569).

Nomenclature

$\boldsymbol{q}$	: Modal coordinate
$\boldsymbol{\xi}$	: Damping matrix
$\boldsymbol{\omega}_0$	: Modal frequency matrix
$\boldsymbol{\Phi}$	: Displacement mode shape matrix
$\boldsymbol{L}$	: Dapping matrix of excitation load
$\boldsymbol{A}$	: Discrete state matrix
$\boldsymbol{B}$	: External excitation input matrix
$\boldsymbol{C}$	: Observation output matrix
$\boldsymbol{D}$	: Direct transmission matrix
$\bar{y}_i$	: Measured mean of each group sensor
y_{ij}	: Measured value
x_k	: Discrete state vector
y_k	: Discrete observation vector
$\boldsymbol{u}_k$	: Discrete external excitation vector
$\boldsymbol{a}_k$	: Process noise of the system
$\boldsymbol{v}_k$	: Measurement noise
$f(\cdot)$	: System state equation
$g(\cdot)$	: System observation equation
$p(\boldsymbol{x}_k \mid \boldsymbol{y}_{1:k})$	: Posterior probability distribution
$p(\boldsymbol{x}_k \mid \boldsymbol{y}_{1:k-1})$	: Prior probability distribution
$p(\boldsymbol{x}_k \mid \boldsymbol{x}_{k-1})$	: Transfer probability density
$\boldsymbol{u}$	: External excitation vector in modal coordinate
$\boldsymbol{h}$	: Drive constant vector
$\boldsymbol{\vartheta}$	: Error vector
$\bar{\boldsymbol{R}}$	: Variance matrix of each group measurement
$\hat{x}$	: Fused estimation state
$\boldsymbol{y}^e$	: Reconstructed response vector
$\boldsymbol{y}^r$	: True response vector
$\boldsymbol{Q}$	: Control coefficient
$\boldsymbol{Ra}$	: Random matrix obeying gaussian distribution

Acronyms

Std	: Standard deviation
RPE	: Relative percentage error
SVPS	: Sampling variance of particle set

References

[1] H. P. Zhu, J. Yu and J. B. Zhang, A summary review and advantages of vibration-based damage identification methods in structural health monitoring, *Engineering Mechanics*, 28 (2) (2011) 1-11+17.

[2] F. L. Huang, X. M. Wang, Z. Q. Chen, C. H. Zeng and X. H. He, Research progress made on the health monitoring for large-type bridges, *China Railway Science*, 26 (2) (2005) 1-7.

[3] J. Wang, S. S. Law and Q. S. Yang, Sensor placement method for dynamic response reconstruction, *Journal of Sound and Vibration*, 333 (9) (2014) 2469-2482.

[4] L. M. Sun, Y. X. Li, W. Zhu and W. Zhang, Structural response reconstruction in physical coordinate from deficient measurements, *Engineering Structures*, 212 (2020) 110484.

[5] J. J. He, X. F. Guan and Y. M. Liu, Structural response reconstruction based on empirical mode decomposition in time domain, *Mechanical Systems and Signal Processing*, 28 (2012) 348-366.

[6] Y. F. Zou, Z. Y. Fu, X. H. He, X. D. Lu, J. S. Yang and S. Zhou, Dynamic response reconstruction method base on empirical mode decomposition and model condensation, *Engineering Mechanics*, 39 (2) (2022) 67-75.

[7] S. S. Law, J. Li and Y. Ding, Structural response reconstruction with transmissibility concept in frequency domain, *Mechanical Systems and Signal Processing*, 25 (3) (2011) 952-968.

[8] J. Li and S. S. Law, Substructural response reconstruction in wavelet domain, *Journal of Applied Mechanics*, 78 (4) (2011) 041010.

[9] D. C. Kammer, Estimation of structural response using remote

sensor locations, *Journal of Guidance, Control and Dynamics*, 20 (3) (1997) 501-508.
[10] R. E. Kalman, A new approach to linear filtering and prediction problems, *Transactions of the ASME-Journal of Basic Engineering*, 82 (Series D) (1960) 35-45.
[11] X. H. Zhang, W. X. Ren and S. E. Fang, Location optimization of dual-type sensors for multi-kind structural response reconstruction, *Journal of Vibration and Shock*, 33 (18) (2014) 26-30.
[12] K. L. Dong, H. Yin and Z. R. Peng, Structural response reconstruction oriented to optimal multi-type sensor placement, *Control Theory and Applications*, 35 (9) (2018) 1339-1346.
[13] R. P. Hu and Y. L. Xu, SHM-based seismic performance assessment of high-rise buildings under long-period ground motion, *Journal of Structural Engineering*, 145 (6) (2019).
[14] X. H. Zhang, Z. B. Wu, S. B. Wu and M. P. Huang, Structural response reconstruction based on moving window Kalman filtering algorithm, *Journal of Vibration and Shock*, 40 (21) (2021) 90-96+105.
[15] S. Q. Hu and Z. L. Jing, Overview of particle filter algorithm, *Control and Decision*, 20 (4) (2005) 361-365+371.
[16] C. Xu, X. X. Wang, S. H. Duan and J. W. Wan, Particle filter tracking algorithm based on error ellipse resampling, *Chinese Journal of Scientific Instrument*, 41 (12) (2020) 76-84.
[17] E. N. Chatzi and A. W. Smyth, Particle filter scheme with mutation for the estimation of time-invariant parameters in structural health monitoring applications, S*tructural Control and Health Monitoring*, 20 (7) (2013) 1081-1095.
[18] S. F. Yuan, H. Zhang, L. Qiu and W. B. Yang, A fatigue crack growth prediction method based on particle filter, *Acta Aeronautica et Astronautica Sinica*, 34 (12) (2013) 2740-2747.
[19] W. B. Yang, S. F. Yuan, L. Qiu and J. Chen, Prediction of fatigue crack propagation based on auxiliary particle filtering, *Journal of Vibration and Shock*, 37 (5) (2018) 114-119+125.
[20] N. J. Gordon, D. J. Salmond and A. F. M. Smith, Novel approach to nonlinear/non-Gaussian Bayesian state estimation, *IEE Proceedings F (Radar and Signal Processing)*, 140 (2) (1993) 107-113.
[21] M. R. Morelande and S. Challa, Manoeuvring target tracking in clutter using particle filters, *IEEE Transactions on Aerospace and Electronic Systems*, 41 (1) (2005) 252-270.
[22] Q. Pan, X. Yu, Y. M. Cheng and H. C. Zhang, Essential methods and progress of information fusion theory, *Acta Automatica Sinica*, 29 (4) (2003) 599-615.
[23] C. Q. Zhong, L. Y. Zhang, S. Y. Yang and W. H. Zhao, Study of grouping weighted fusion algorithm for multi-sensor, *Journal of Dalian University of Technology*, 42 (2) (2002) 242-245.
[24] L. Y. Zhang, L. Zhang and D. Li, Grouping weighted fusion algorithm for multi-sensor and its optimal grouping principle, *Chinese Journal of Scientific Instrument*, 29 (1) (2008) 200-205.
[25] Y. X. Lv and X. H. Gu, Filtering algorithm for multi-microphones based on wavelet multi-scale information fusion, *Chinese Journal of Scientific Instrument*, 33 (4) (2012) 788-794.
[26] Z. R. Peng, Z. H. Wang, H. Yin, Y. Bai and K. L. Dong, A new Bayesian finite element model updating method based on information fusion of multi-source markov chains, *Journal of Sound and Vibration*, 526 (2022) 116811.
[27] R. J. Mu and N. G. Cui, Theoretical and simulation research on optimizing information fusion method for multi-sensor, *Chinese Journal of Scientific Instrument*, 27 (6) (2006) 326-328.
[28] L. P. Gao, H. N. Huang and D. M. Xu, On data fusion using maximum likelihood method and its application to underwater robot, *Journal of Northwestern Polytechnical University*, 17 (2) (1999) 306-310.

Yonghe Shi was born in Shaanxi Province in China. She received the bachelor's degree in industrial engineering from Lanzhou Jiaotong University, Lanzhou, China, in 2019, where she is currently pursuing the master's degree in vehicle engineering. Her main research interests include modal analysis, load identification, and structural response reconstruction.

Hong Yin received the bachelor's degree in mechanical engineering from Lanzhou Jiaotong University, Lanzhou, China, in 2000, and where she received the Ph.D. degree in mechanical engineering, in 2019. She participated in three projects of the National Natural Science Foundation of China and her major research fields include modal analysis, structural response reconstruction, and signal processing.

Zhenrui Peng received the bachelor's degree in mechanical engineering from Lanzhou Jiaotong University, Lanzhou, China, in 1995, and the Ph.D. degree in control science and engineering from Zhejiang University, Hangzhou, China, in 2007. He presided over three projects of the National Natural Science Foundation of China and published over 90 papers up to now, and over 30 papers have been indexed by SCI, EI, and ISTP. His major research fields include fault diagnosis of mechanical equipment, finite element model updating, and structural response reconstruction.

Zenghui Wang received the bachelor's degree in mechanical engineering from Lanzhou Jiaotong University, Lanzhou, China, in 2019, and where he received the master's degree in mechanical engineering, in 2022. He is currently a Ph.D. candidate in the School of Mechanical Engineering at Xi'an Jiaotong University, Xi'an, China. His major research fields include uncertainty finite element model updating, Bayesian inference and digital twin.

Yu Bai received his bachelor's degree in mechanical engineering from Shandong University of Technology, Zibo, China, in 2009, and where he received his master's degree in agricultural mechanization engineering in 2011. He is currently pursuing his Ph.D. degree in the School of Mechanical Engineering at Lanzhou Jiaotong University, Lanzhou, China. His main research areas include finite element model updating and intelligent optimization.